Baroclinic–Barotropic Instabilities of the Gulf Stream Extension

A. A. DIMAS* AND G. S. TRIANTAFYLLOU

The Benjamin Levich Institute for Physico-Chemical Hydrodynamics and Department of Mechanical Engineering, The City College of CUNY, New York, New York

(Manuscript received 22 December 1993, in final form 19 July 1994)

ABSTRACT

In this paper, the baroclinic–barotropic instability of the Gulf Stream is studied numerically. The quasigeostrophic potential vorticity equation is linearized around the mean flow, which is modeled using data from field measurements in the Gulf Stream off Cape Hatteras. The perturbation around the mean flow is decomposed into waves along the streamwise direction using a Fourier transformation in space and a Laplace transformation in time. For each wave, an eigenvalue problem is obtained, which is solved numerically to yield the frequency as a function of the wavenumber. The instability is of the convective type, in the sense that any localized perturbation will propagate out of any fixed region in space in finite time. External noise can, however, drive the instability creating spatially growing waves. The spatial growth rates of the waves are computed as a function of their frequency using an iterative procedure and are found to be in good agreement with growth rates from field measurements. Visualizations of the computed spatial instability modes show strong resemblance with the meandering patterns observed in pictures of the Gulf Stream.

1. Introduction

Downstream of Cape Hatteras, the path of the Gulf Stream is characterized by the presence of wavy perturbations known as Gulf Stream meanders, which are due to large-scale instabilities of the mean flow in the current. Linear instability theory can give a good description of the first stages of the formation of meanders. The problem is approached with the aid of the quasigeostrophic assumption (Pedlosky 1987). The limitations of this approach to the Gulf Stream are well known but are less important in this case because the effect of the presence of the shore to the isopycnals distribution across the stream is minimal downstream of Cape Hatteras (for example, see Joyce et al. 1988).

The instability of the Gulf Stream has been extensively studied in the past. Thus, Johns (1988) modeled the dynamics of the Gulf Stream as a temporal baroclinic instability and Hogg (1976) as a spatial baroclinic instability. Baroclinic instabilities are due to the vertical shear of the current and the density gradient of the fluid. Hart (1974) studied mixed (baroclinic–barotropic) temporal instabilities of an idealized two-layer model of ocean currents and revealed the importance of the barotropic contribution, while Holland and Haidvogel (1980) studied mixed temporal instabilities in an idealized two-layer model of the Gulf Stream and report that up to 10% of eddy energy is derived from barotropic contribution. Barotropic instabilities are associated with the horizontal shear of the current. Their predictions, though, about maximum temporal growth rate and wavenumber range of unstable waves underestimate field measurements (Watts and Johns 1982; Tracey and Watts 1986) by 50%, due to the simplifying two-layer assumption about the mean flow. Rossby (1987) studied the transfer of energy between the mean and fluctuating fields in the Gulf Stream off Cape Hatteras and found that although the baroclinic conversion term was the largest, the barotropic term is also important, especially close to the ocean surface. Xue and Mellor (1993) studied mixed temporal instabilities and Luther and Bane (1985) studied mixed spatial instabilities of a realistic two-dimensional model of the Gulf Stream upstream of Cape Hatteras over the continental slope, where the influence of topography on the instability is important, and they also report significant barotropic contributions. Farrell and Moore (1992) have recently modeled the instabilities of the Gulf Stream as a transient growth problem.

In this paper, a two-dimensional model of the basic-state zonal flow is considered by using field measurements of the velocity and density distribution in the Gulf Stream after it leaves the North American coast. The instability of the current is thus two-dimensional, and barotropic effects can significantly alter the character of the instability. Moreover, the instability analysis is done within the framework of absolute versus

* Current affiliation: Department of Mechanical Engineering, University of Maryland, College Park, Maryland.

Corresponding author address: Dr. A. A. Dimas, Department of Mechanical Engineering, University of Maryland at College Park, College Park, MD 20742-3035.

convective distinction [similar to the baroclinic instabilities of two-layer models considered by Merkine (1977) and Pierrehumbert (1984)], which is fundamental in the study of effectively unbounded media. In this context, emphasis is given to the study of the Gulf Stream dynamics as a spatial instability rather than a temporal one.

2. Formulation

We consider the evolution of small perturbations around the mean flow in an ocean current. The basic equation is the quasigeostrophic potential vorticity equation linearized about the basic-state zonal flow (see Pedlosky 1987 for the derivation):

$$\left(\frac{\partial}{\partial t} + U\frac{\partial}{\partial x}\right)q + \frac{\partial \Psi}{\partial x}Q_y = 0, \tag{1}$$

where

$$q = \frac{\partial^2 \Psi}{\partial x^2} + \frac{\partial^2 \Psi}{\partial y^2} + \frac{\partial}{\partial z}\left(\frac{1}{S}\frac{\partial \Psi}{\partial z}\right), \quad S = \frac{N^2}{f^2}\frac{D^2}{L^2}, \tag{2}$$

and

$$Q_y = \frac{\partial Q}{\partial y} = \beta - \frac{\partial^2 U}{\partial y^2} - \frac{\partial}{\partial z}\left(\frac{1}{S}\frac{\partial U}{\partial z}\right). \tag{3}$$

In the above equations, $U(y, z)$ is the velocity profile of the mean zonal flow, $\Psi(x, y, z, t)$ the streamfunction, $q(x, y, z, t)$ the potential vorticity of the perturbation flow, $Q(y, z)$ the potential vorticity of the mean zonal flow, f the Coriolis parameter, β the northward variation of the Coriolis parameter, and $N(z)$ is the Brunt–Väisälä frequency. Equations (1)–(3) have been nondimensionalized: lengths in the streamwise x direction and spanwise y direction with respect to L, which is the typical length scale of the basic state in the y direction, and lengths in the vertical z direction with respect to D, which is the total depth of the system, and velocities with respect to U_c, which is the maximum velocity of the basic-state zonal flow.

The boundary conditions at the ocean surface ($z = 1$) and at the bottom ($z = 0$) require that there is no flow normal to the boundary. Consequently, the boundary condition at both $z = 1$ and $z = 0$ is

$$\left(\frac{\partial}{\partial t} + U\frac{\partial}{\partial x}\right)\frac{\partial \Psi}{\partial z} - \frac{\partial U}{\partial z}\frac{\partial \Psi}{\partial x} = 0. \tag{4}$$

Because of the symmetry of U and Q_y around $y = 0$, we can separately consider perturbations with a streamfunction that is symmetric or antisymmetric around $y = 0$. The former corresponds to the so-called sinuous mode and the latter to the varicose mode. For a symmetric perturbation, the boundary condition at $y = 0$ is

$$\frac{\partial \Psi}{\partial y} = 0, \tag{5}$$

whereas for an antisymmetric perturbation, the boundary condition at $y = 0$ is

$$\Psi = 0. \tag{6}$$

Finally, as $y \to +\infty$, the condition is that the perturbation flow vanishes; in other words, we have that

$$\Psi \to 0. \tag{7}$$

Assuming that the flow is homogeneous in the streamwise direction, we can decompose the perturbation into waves by taking the Fourier transform in x and the Laplace transform in time. Equivalently, we can substitute the following expression into (1):

$$\Psi(x, y, z, t) = \Phi(y, z)e^{i(kx-\omega t)}, \tag{8}$$

where k is the Fourier transform variable, which is the wavenumber in the x direction, ω is the Laplace transform variable, which is the frequency, and Φ is the Fourier–Laplace transform of Ψ. Then, Eq. (1) becomes

$$\left(U - \frac{\omega}{k}\right)\left[-k^2\Phi + \frac{\partial^2 \Phi}{\partial y^2} + \frac{\partial}{\partial z}\left(\frac{1}{S}\frac{\partial \Phi}{\partial z}\right)\right] + \Phi\left[\beta - \frac{\partial^2 U}{\partial y^2} - \frac{\partial}{\partial z}\left(\frac{1}{S}\frac{\partial U}{\partial z}\right)\right] = 0. \tag{9}$$

The boundary conditions (4) at the lower ($z = 0$) and upper ($z = 1$) boundaries become

$$\left(U - \frac{\omega}{k}\right)\frac{\partial \Phi}{\partial z} - \frac{\partial U}{\partial z}\Phi = 0. \tag{10}$$

The other boundary conditions become

$$\frac{\partial \Phi}{\partial y} = 0 \tag{11}$$

for the symmetric mode at $y = 0$, and

$$\Phi = 0 \tag{12}$$

for the antisymmetric mode at $y = 0$, while as $y \to +\infty$, the condition is

$$\Phi \to 0. \tag{13}$$

For the numerical solution of the above equations, a centered three-point finite-difference scheme is used. In the y direction, the domain is truncated at a point $y = B$ where U and its derivatives $\partial U/\partial y$ and $\partial^2 U/\partial y^2$ all become very small. Furthermore, assuming that at this point $\partial \Phi/\partial z$ will also be very small, Eq. (9) becomes

$$k^2\Phi - \frac{\partial^2 \Phi}{\partial y^2} = 0 \tag{14}$$

since β is much smaller than the typical k^2 considered in this study.

In this form, the equation has an analytic solution, which satisfies the boundary conditions in the other

direction. Therefore, at $y = B$, we apply the truncation condition:

$$\Phi \sim e^{-ky}. \tag{15}$$

3. Modeling of the basic state

We consider the stability of the mean flow in the Gulf Stream Extension off Cape Hatteras. The basic state has been modeled using the data of Halkin and Rossby (1985), Robinson et al. (1986), and Johns (1988).

For the velocity field $U(z, y)$ of the zonal flow, we used the data shown in Figs. 3a, 3c, and 8b of Halkin and Rossby (1985) and Fig. 1a of Johns (1988). We consider that the velocity can be written as

$$U(y, z) = U_c U^y(y) U^z(z), \tag{16}$$

where $U_c = 1.8$ m s^{-1} is the maximum velocity of the basic state, U^y is the function that describes the y variation of the velocity profile, and U^z is the function that describes the z variation of the velocity profile.

For the z variation, we use the expression:

$$U^z(z) = 0.139z + 0.861 \exp[-a(z-1)^2], \tag{17}$$

where $z = 0$ corresponds to the lower boundary, $z = 1$ corresponds to the upper boundary, and $a = 40$ is a fitting parameter. The dimensional depth of the system is $D = 4$ km.

For the y variation, we use the expression

$$U^y(y) = \exp(-y^2), \tag{18}$$

where the nondimensional point $y = 1$ corresponds to a dimensional length L that characterizes the spanwise scale of the Gulf Stream. Physically, $2L$ is the half-width of the Gulf Stream Extension (see definition sketch in Fig. 1). For the best possible fitting of our velocity profile (16) to the data shown in Fig. 8b of the paper by Halkin and Rossby (1985), L should take values between 40 and 60 km. Velocity contour plots of the profile (16) for $L = 40$ km, $L = 50$ km, and $L = 60$ km are shown in Fig. 2. The best fitting is obtained for $L = 50$ km.

Since the velocity profile is modeled as a separable function of y and z, the density field $\rho(y, z)$ will also be a separable function of y and z due to the thermal wind balance between velocity and density field. Therefore, the Brunt–Väisälä frequency

$$N^2 = -\frac{g}{\rho}\frac{\partial \rho}{\partial z} \tag{19}$$

will be a function of z only, and as a model we use the profile shown in Fig. 1a of the paper by Robinson et al. (1986). We fit these data with the expression

$$N^2(z) = \sum_{i=1}^{4} a_i \exp[-b_i(z - c_i)^2], \tag{20}$$

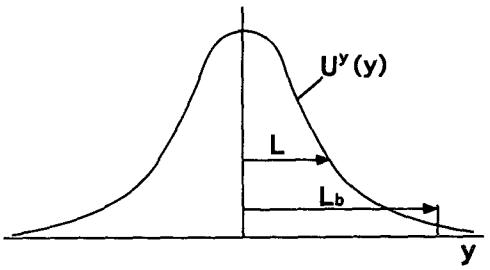

FIG. 1. Definition sketch for the variation of the mean velocity profile in the y direction.

where N^2 is given in 10^{-4} s^{-2}, z is nondimensional ($0 \leq z \leq 1$), and $a_1 = 0.9369$, $a_2 = 0.1611$, $a_3 = -0.0242$, $a_4 = 0.00456$; $b_1 = 544.2$, $b_2 = 50.8$, $b_3 = 272.1$, $b_4 = 90.7$; $c_1 = 1$, $c_2 = 0.825$, $c_3 = 0.6955$, $c_4 = 0.5485$ are the fitting constants. The fitting of the density variation by the above analytic expression is quite good: the rms error was less than one percent. The profile is shown in Fig. 3.

Finally, since these data are obtained at a latitude of 35°N, the Coriolis parameter is $f^2 = 0.7 \times 10^{-8}$ s^{-2}, and the northward variation of the Coriolis parameter is $\beta = 0.19 \times 10^{-10}$ m^{-1} s^{-1}. Based on these numbers, the potential vorticity gradient Q_y of the mean flow can be computed from Eq. (3), and its vertical distribution at $y = 0$ is shown in Fig. 4.

4. Results

a. Temporal instability

Equation (9) subject to the boundary conditions defines an eigenvalue problem for the frequency ω once the wavenumber k is specified (and vice versa); in other words, it constitutes the dispersion relation of the system. We will denote this relation between ω and k as $D(\omega, k) = 0$. The eigenvalue problem for ω is solved numerically. More specifically, the computational domain is truncated in the y direction (a nondimensional width $B = 4$ is used), and Eq. (9) is discretized using a centered three-point finite-difference scheme to approximate the derivatives of Φ. Typical size of the two-dimensional grid is 40 points in the y direction and 100 points in the z direction. Then, a generalized algebraic eigenvalue problem is obtained for ω, which is solved using a standard QZ algorithm.

A simpler approach, used in the past in several studies (for instance, see Johns 1988), is to reduce the partial differential equation (9) to an ordinary differential equation. To this purpose, the basic-state velocity profile is assumed to depend only on z, $U(z) = U_b U^z(z)$, and it is taken to be equal to the average of the actual velocity distribution $U(y, z)$ over some length $2L_b$ in the y direction, so that the total mass transport does not change. Physically, $2L_b$ corresponds roughly to the width of the Gulf Stream Extension (see

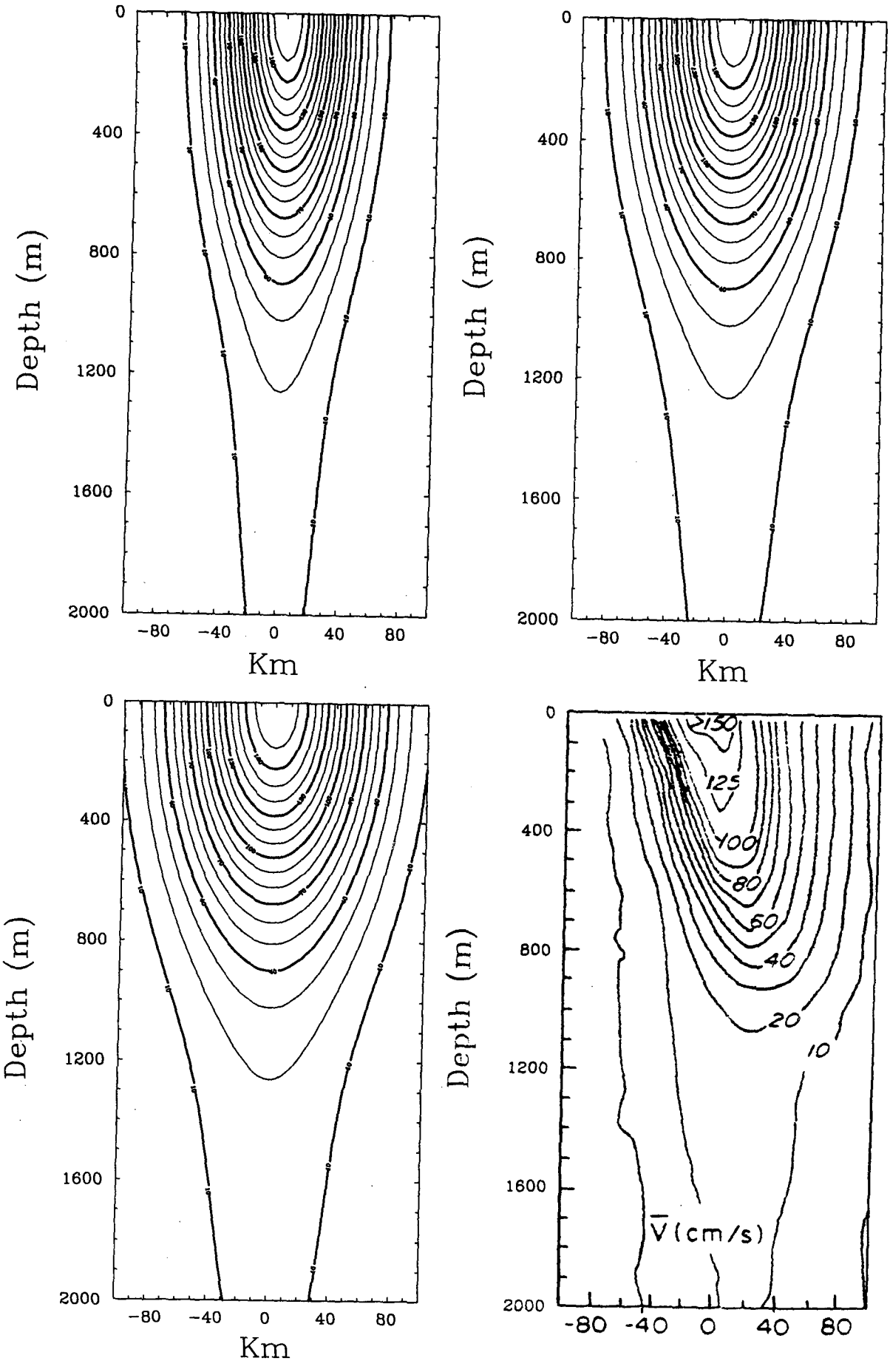
Depth (m)
0
400
800
1200
1600
2000
-80
-40
0
40
80
Km
150
125
100
80
60
40
20
10
$\bar{V}$(cm/s)

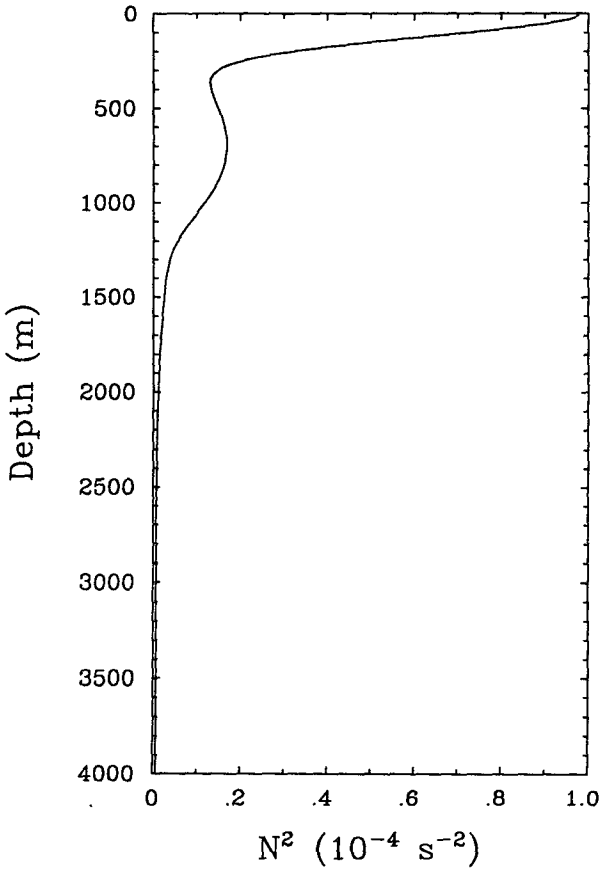

FIG. 3. The Brunt–Väisälä profile. The standard deviation for the fitting is less than 1%.

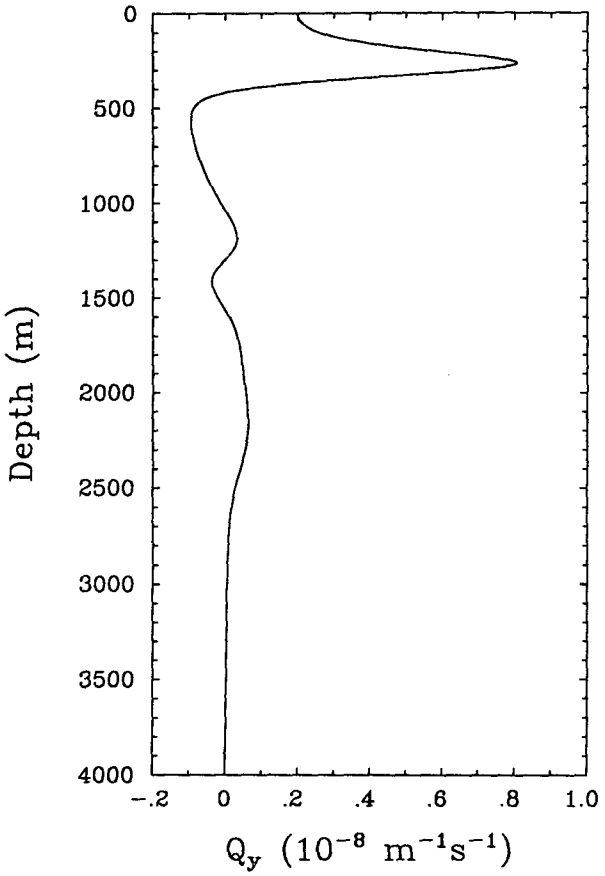

FIG. 4. Vertical distribution of the basic-state potential vorticity gradient at $y = 0$.

Fig. 1), and typical values vary between $L_b = 75$ km and $L_b = 100$ km (we note that L_b is approximately $2L$ of our model). Therefore, the maximum velocity U_b is given by the equation:

$$U_b L_b = U_c L \int_0^\infty U^y(y)dy = U_c L \frac{\sqrt{\pi}}{2}, \quad (21)$$

where U^y, U^z are the same functions that describe the velocity profile (16).

This approach assumes that the instability of the flow is dominated by its baroclinic character, while the barotropic effect is minimal. The perturbation field is confined in a channel of width $2L_b$ and is given by the expression

$$\Psi(x, y, z, t) = \Phi(z) \cos\left(\frac{\pi y}{2}\right) e^{i(kx-\omega t)}. \quad (22)$$

This choice imposes the condition that $\Psi = 0$ at $y = \pm 1$ ($\pm L_b$ in dimensional form). We will use this simpler baroclinic instability model for comparison purposes in order to assess the importance of the barotropic effect.

For the two-dimensional velocity profile (16) with $L = 40$ km, $L = 50$ km, and $L = 60$ km, the temporal growth rate ω_i is shown as a function of the wavenumber k_r in Fig. 5. In Fig. 6, ω_i is plotted as a function of the frequency ω_r. Figures 5 and 6 show that the baroclinic–barotropic instability is characterized by the presence of two regions of unstable waves with overlapping wavenumber and frequency ranges. The results from the corresponding baroclinic instability analysis with $L_b = 75$ km and $L_b = 100$ km are also shown for comparison, together with measurements by Tracey and Watts (1986) and Watts and Johns (1982). In

FIG. 2. Velocity contour plot of the basic-state zonal flow: (a) is the fitting with $L = 40$ km, (b) is the fitting with $L = 50$ km, (c) is the fitting with $L = 60$ km, and (d) is the measured profile (reproduction of Fig. 8b of Halkin and Rossby 1985). The velocity contour levels are given in cm s^{-1}.

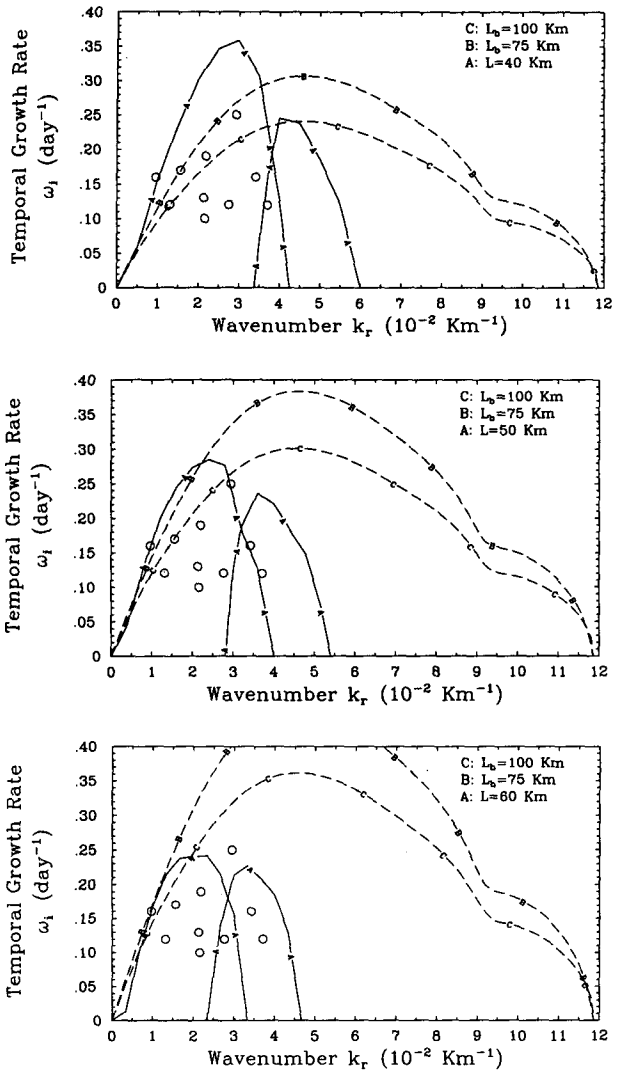

FIG. 5. The temporal growth rate variation with respect to the wavenumber for different values of L. The solid line represents the baroclinic–barotropic instability, the dashed line represents the baroclinic instability (B corresponds to L_b = 75 km, C corresponds to L_b = 100 km), and the circles represent the measurements.

those figures, the results for the sinuous mode (symmetric streamfunction mode) are shown, which was always found to be more unstable than the varicose mode. In comparison with the temporal instability results upstream of Cape Hatteras in the Charleston Bump region (Xue and Mellor 1993), we get larger wavelengths and smaller growth rates for the most unstable waves. More specifically, our wavelengths are 250–300 km and our growth rates are 0.25–0.35 day^{-1}, while Xue and Mellor (1993) get wavelengths of 185–225 km and growth rates of 0.30–0.55 day^{-1}. These differences are consistent with the observations of the Gulf Stream, which show an increase of the wavelength of the instability downstream of Cape Hatteras.

For the baroclinic–barotropic instability with L = 50 km, the variation of the temporal growth rate with respect to the wavenumber and the frequency of the unstable waves is in reasonably good agreement with the measurements, considering the fact that the measurements have an uncertainty level between 25% and 50%, but the wavenumber range of the measurements is overpredicted by 35%, whereas the corresponding frequency range is overpredicted by a factor of 2. For L = 60 km, the maximum baroclinic–barotropic instability growth rate is within 10% of the measurement, while the model overpredicts the wavenumber range by 20%, and the frequency range by a factor of 2. For L = 40 km, the model overpredicts the

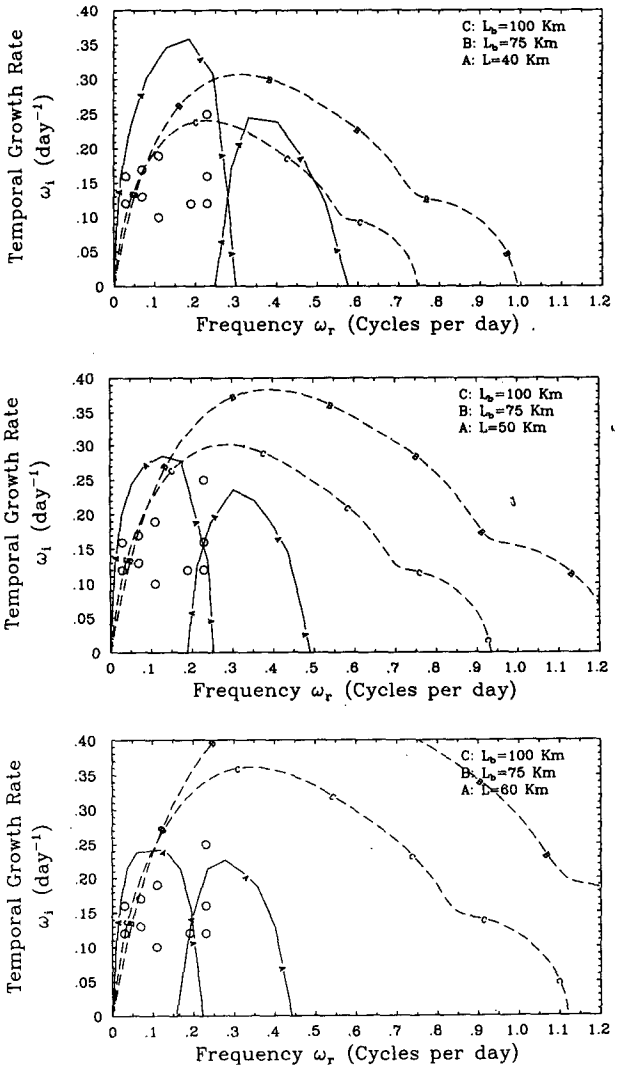

FIG. 6. The temporal growth rate variation with respect to the frequency for different values of L. The solid line represents the baroclinic–barotropic instability, the dashed line represents the baroclinic instability (B corresponds to L_b = 75 km, C corresponds to L_b = 100 km), and the circles represent the measurements.

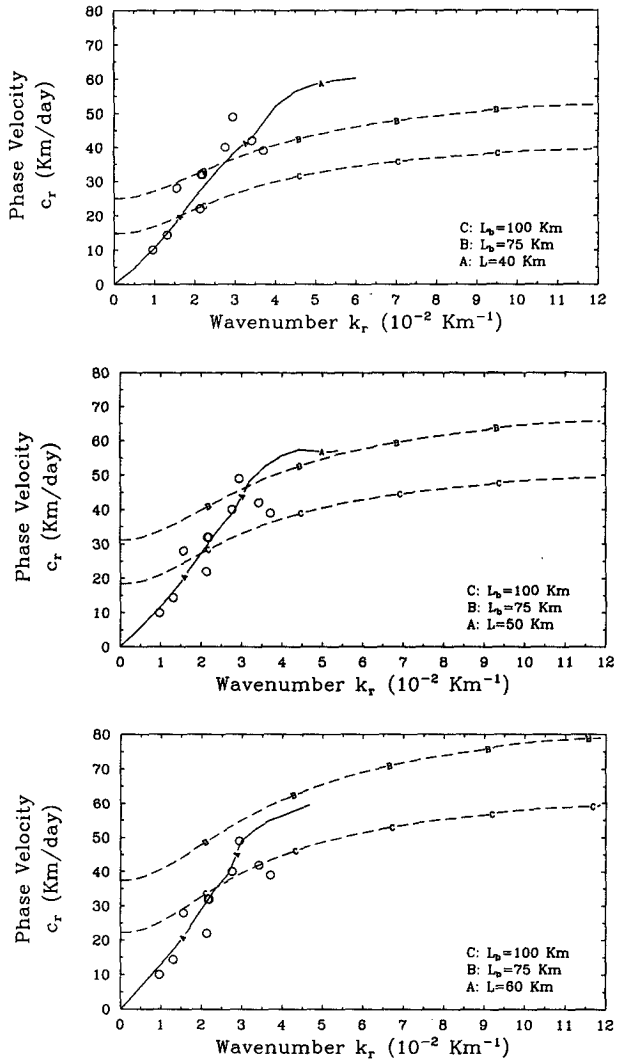

FIG. 7. The phase velocity variation with respect to the wavenumber for different values of L. The solid line represents the baroclinic–barotropic instability, the dashed line represents the baroclinic instability (B corresponds to L_b = 75 km, C corresponds to L_b = 100 km), and the circles represent the measurements.

maximum growth rate by about 30%, the wavenumber range by 50%, and the frequency range by a factor of 2.5. Therefore, the predictions for the growth rates of the baroclinic–barotropic instability decrease as L increases from 40 to 60 km, and the best agreement with the measurements is achieved for L between 50 and 60 km. The decrease of the growth rates is attributed to the decrease of the barotropic effect as the shear of the mean flow in the y direction becomes weaker with the increase of L.

The growth rates predicted by the baroclinic instability model, on the other hand, exhibit the opposite trend as L increases than those of the baroclinic–barotropic model due to the absence of the barotropic effect. The growth rates of the baroclinic instability increase

TABLE 1. Barotropic and baroclinic contribution in percent to the growth of the energy of the instability for different values of L.

	Contribution	
L (km)	Barotropic	Baroclinic
40	43	57
50	26	74
60	10	90

as L increases from 40 to 60 km, and decrease as L_b increases from 75 to 100 km. It is worth noting, however, that even in the best case (L = 40 km and L_b = 100 km), where the baroclinic analysis gives a good prediction for the maximum growth rate, both the wavenumber and frequency ranges are overpredicted by a factor of 3. Results for the phase velocity as a function of the wavenumber are shown in Fig. 7. Again, the baroclinic–barotropic results are in better agreement with the measurements than the baroclinic ones.

The barotropic effect is therefore more important at smaller values of L, as it can be anticipated intuitively (see also Holland and Haidvogel 1980). The barotropic effect on the instability can also be assessed by computing the rate of change of the energy of the perturbation flow and by partitioning it into barotropic and baroclinic effects. The equation for the rate of change the energy of the perturbation is (Pedlosky 1987)

$$\frac{dE}{dt} = \int_0^D dz \int_{-\infty}^{+\infty} dy \left(\overline{\frac{\partial \Psi}{\partial x}\frac{\partial \Psi}{\partial y}}\frac{\partial U}{\partial y} + \overline{\frac{\partial \Psi}{\partial x}\frac{\partial \Psi}{\partial z}}\frac{1}{S}\frac{\partial U}{\partial z} \right), \tag{23}$$

where

$$E = \frac{1}{2}\int_0^D dz \int_{-\infty}^{+\infty} dy \left(\overline{\left(\frac{\partial \Psi}{\partial x}\right)^2} + \overline{\left(\frac{\partial \Psi}{\partial y}\right)^2} + \frac{1}{S}\overline{\left(\frac{\partial \Psi}{\partial z}\right)^2} \right) \tag{24}$$

is the energy of the perturbation flow and the overbars indicate averaging in the x direction. The right-hand

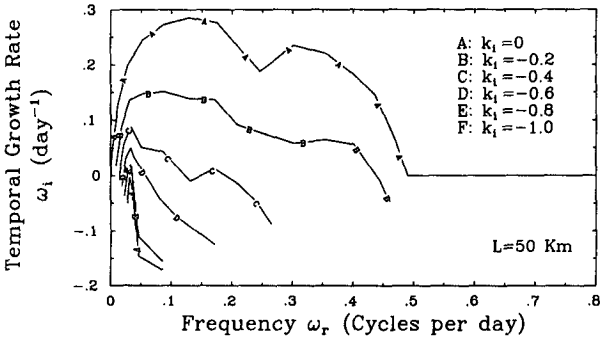

FIG. 8. The mapping of lines parallel to the k-real axis through the dispersion relation into the complex ω plane for the baroclinic–barotropic instability with L = 50 km.

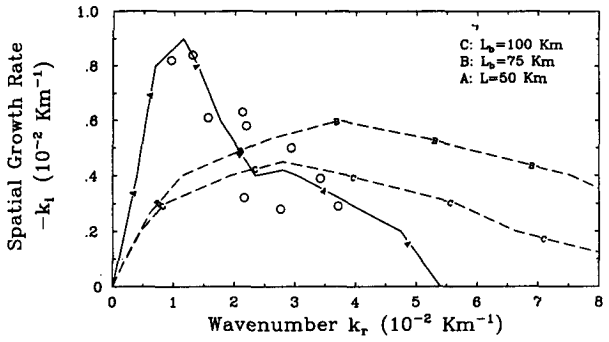

FIG. 9. The spatial growth rate variation with respect to the wavenumber. The solid line represents the baroclinic–barotropic instability, the dashed line represents the baroclinic instability, and the circles represent the measurements.

side of Eq. (23) indicates that there are two terms that contribute to the growth of the perturbation energy. The first one depends on the horizontal shear of the mean flow and therefore is associated with barotropic effects, while the second one depends on the vertical shear of the mean flow as well as the density gradient and therefore it is associated with baroclinic effects.

For the baroclinic–barotropic instability with the maximum temporal growth rate, the contribution of the barotropic term to the right-hand side of Eq. (23) and the contribution of the baroclinic term are summarized in Table 1 for different values of L.

Therefore, the barotropic contribution is larger for smaller values of L, but as can be seen in Figs. 5 and 6, it seems to be always important for the frequencies and wavenumbers of the unstable waves.

b. *Spatial growth*

As the current is effectively infinite along the streamwise direction, the question arises as to whether the instability is of the absolute or the convective type. The instability is absolute when an initially localized excitation grows and spreads upstream and downstream leading to a motion growing in time at any location in space. The instability is, on the other hand, convective if any localized excitation propagates away from its initial position leading to motions decaying in time at any fixed location. To distinguish between the two, one has to determine the pinching double roots of the dispersion relation (Bers 1983). If any such double root has a complex frequency with a positive imaginary part, the instability is absolute; otherwise, the instability is convective. To see whether any such double root exists, the procedure suggested in Triantafyllou et al. (1986) was followed: lines parallel to the k-real axis are mapped through the dispersion relation into the complex ω plane. A pinching double root with a positive imaginary part will appear in the ω plane as a cusp singularity lying below the map of the k-real axis. This mapping, for the baroclinic–barotropic instability with L = 50 km, was constructed in Fig. 8, where it can be seen that there is no such singularity, and we conclude that the instability is convective.

Convective instabilities are very sensitive to any background noise in the system. In fact, a wideband noise drives a convective instability creating a spatially growing response. Asymptotically for large x, the fastest growing wave in space dominates. Consequently, a better way to model the Gulf Stream dynamics is as a spatial instability of the mean flow. To this purpose, the dispersion relation has to be solved to yield solutions with real frequencies and complex wavenumbers. This has been done using an iterative procedure. The imaginary part of the complex wavenumber is the growth rate in space. Spatial growth rates $-k_i$ as a function of the wavenumber are shown in Fig. 9 both for the baroclinic–barotropic and the baroclinic insta-

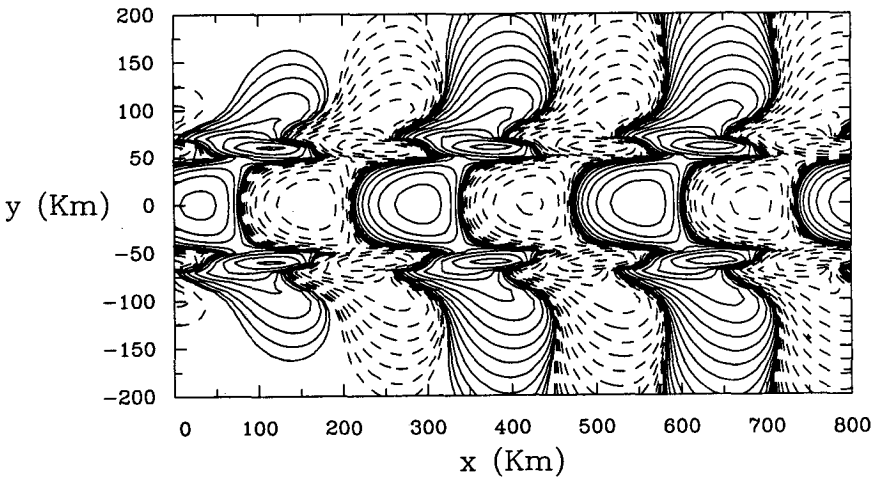

FIG. 10. Contour plot of the vorticity of the perturbation flow at the ocean surface. Solid lines indicate negative (counterclockwise) vorticity and dashed lines indicate positive (clockwise) vorticity.

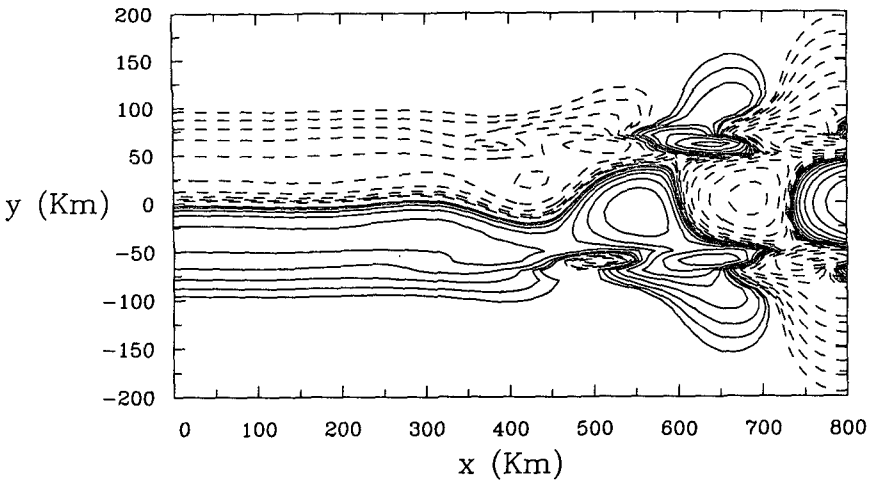

FIG. 11. Contour plot of the vorticity of the total flow at the ocean surface. Solid lines indicate negative (counterclockwise) vorticity and dashed lines indicate positive (clockwise) vorticity.

bilities. As was the case with the temporal growth rates, the baroclinic model overpredicts the wavenumber range of unstable waves by a factor of 3, while the predictions of the baroclinic–barotropic model are very close to the measurements of Tracey and Watts (1986). The predictions of the spatial growth rates are also quite good for the baroclinic–barotropic instability.

Finally, from the computation with $L = 50$ km, the vorticity of the spatial eigenmode of the instability with the maximum spatial growth rate is shown in Fig. 10. The amplitude of the mode cannot be determined within linear theory. To obtain a visual picture of the growing mode, an amplitude of 1% of the mean flow was assumed at $x = 0$, and the vorticity of the mean flow was added (Fig. 11). The visualization is indeed reminiscent of satellite pictures of the Gulf Stream, although a direct comparison is not possible, since satellites do not measure vorticity.

5. Conclusions

The stability of the Gulf Stream has been analyzed numerically by including baroclinic and barotropic effects, and the computed growth rates, frequencies, and wavenumbers were found to be in good agreement with the measurements of Watts and Johns (1982) and Tracey and Watts (1986). It has also been shown through comparison with measurements and numerical flow visualizations that the spatial instability model is the appropriate one for the Gulf Stream instability (which is of the convective type).

Significant differences were found between the results obtained from the baroclinic–barotropic model and those obtained from the simpler baroclinic model. The differences were found to be largest for narrow domains, where barotropic effects become dominant. Even for wide domains, however, for which the baroclinic model predicts the growth rates of the instability with reasonable accuracy, barotropic effects are essential in determining the frequency and wavenumber range of unstable waves. More specifically, for widths typical of the Gulf Stream, the wavenumber range of unstable waves predicted by the baroclinic–barotropic analysis differs by a factor of as much as 3, compared to the one obtained from a purely baroclinic analysis, and agrees much better with measurements obtained from field experiments.

The amplitude of the instability waves cannot be predicted from linear theory only. It is clear, however, from the results of the linear analysis that the waves grow and saturate in space. It will be interesting to investigate whether the saturation can be modeled using an amplitude equation (like the Stuart–Landau equation in space).

Acknowledgments. The financial support of the Office of Naval Research is gratefully acknowledged.

REFERENCES

Bers, A., 1983: Space-time evolution of plasma instabilities: Absolute and convective. *Handbook of Plasma Physics,* M. N. Rosenbluth and R. Z. Sagdeev, Eds., Van Nostrand, 451–517.

Farrell, B. F., and A. M. Moore, 1992: An adjoint method for obtaining the most rapidly growing perturbation to oceanic flows. *J. Phys. Oceanogr.,* **22,** 338–349.

Halkin, D., and T. Rossby, 1985: The structure and transport of the Gulf Stream at 73°W. *J. Phys. Oceanogr.,* **15,** 1439–1452.

Hart, J. E., 1974: On the mixed stability problem for quasi-geostrophic ocean currents. *J. Phys. Oceanogr.,* **4,** 349–356.

Hogg, N. G., 1976: On spatially growing baroclinic waves in the ocean. *J. Fluid Mech.,* **78,** 217–235.

Holland, W. R., and D. B. Haidvogel, 1980: A parameter study of the mixed instability of idealized ocean currents. *Dyn. Atmos. Oceans,* **4,** 185–215.

Johns, W. E., 1988: One-dimensional baroclinically unstable waves on the Gulf Stream potential vorticity gradient near Cape Hatteras. *Dyn. Atmos. Oceans,* **11,** 323–350.

Joyce, T. M., C. Wunsch, and S. D. Pierce, 1986: Synoptic Gulf Stream velocity profiles through simultaneous inversion of hydrographic and acoustic Doppler data. *J. Geophys. Res.*, **91,** 7573–7585.

Luther, M. E., and J. M. Bane, 1985: Mixed instabilities in the Gulf Stream over the continental slope. *J. Phys. Oceanogr.*, **15,** 3–23.

Merkine, L., 1977: Convective and absolute instability of baroclinic eddies. *Geophys. Astrophys. Fluid Dyn.*, **9,** 129–157.

Pedlosky, J., 1987: *Geophysical Fluid Dynamics.* Springer-Verlag, 710 pp.

Pierrehumbert, R. T., 1984: Local and global baroclinic instability of zonally varying flow. *J. Atmos. Sci.*, **41,** 2141–2162.

Robinson, A. R., M. A. Spall, and N. Pinardi, 1986: Gulf Stream simulations and the dynamics of ring and meander processes. *J. Phys. Oceanogr.*, **18,** 1811–1853.

Rossby, T., 1987: On the energetics of the Gulf Stream at 73°W. *J. Mar. Res.*, **45,** 59–82.

Tracey, K. L., and D. R. Watts, 1986: On Gulf Stream meander characteristics near Cape Hatteras. *J. Geophys. Res.*, **91,** 7587–7602.

Triantafyllou, G. S., M. S. Triantafyllou, and C. Chryssostomidis, 1986: On the formation of vortex streets behind stationary cylinders. *J. Fluid Mech.*, **170,** 461–477.

Watts, D. R., and W. E. Johns, 1982: Gulf Stream meanders: Observations on propagation and growth. *J. Geophys. Res.*, **87,** 9467–9476.

Xue, H., and G. Mellor, 1993: Instability of the Gulf Stream Front in the South Atlantic Bight. *J. Phys. Oceanogr.*, **23,** 2326–2350.